Compton-Scattering Total Cross Section at Next-to-Next-to-Leading Order and Resummation of Leading Logarithms

Hai Tao Li,[1,*] Yan-Qing Ma,[2,3,†] Cheng-Tai Tan,[2,‡] Jian Wang,[1,3,§] and Hong-Fei Zhang[4,‖]
[1]School of Physics, Shandong University, Jinan, Shandong 250100, China
[2]School of Physics, Peking University, Beijing 100871, China
[3]Center for High Energy Physics, Peking University, Beijing 100871, China
[4]College of Big Data Statistics, Guizhou University of Finance and Economics, Guiyang 550025, China

(Received 20 November 2025; accepted 23 December 2025; published 13 January 2026)

Compton scattering is a fundamental process in QED with broad applications, yet its theoretical description at high energies is challenged by substantial next-to-leading order corrections arising from double-logarithmic enhancements. To address this, we report the first calculation of the next-to-next-to-leading order (NNLO) total cross section with full electron mass dependence. Our analysis reveals that the NNLO correction, albeit still containing double logarithms, is numerically small due to a suppressing prefactor. By identifying the origin of these logarithms in a kinematic regime featuring a Glauber electron exchange, we successfully resum the leading logarithmic series to all orders, obtaining a compact result in terms of a modified Bessel function. The all-order structure reveals a suppression mechanism, which explains the rapid convergence of higher-order contributions. The combination of our NNLO calculation and all-orders resummation delivers a reliable and precise prediction, poised to serve the needs of high-precision experiments in the foreseeable future.

DOI: 10.1103/k2mk-mffq

Introduction—Compton scattering, namely the scattering of a photon off an electron, dates back more than a century to Compton's observation of the wavelength shift of photons after interacting with electrons [1], a discovery that played a pivotal role in the development of quantum mechanics. Today, Compton scattering is widely exploited across a broad range of applications, from medical physics [2] and x-ray and gamma-ray astronomy [3] to studies of fundamental quantum phenomena [4]. In the context of high-energy particle colliders—including the Future Circular Collider, the International Linear Collider, the Circular Electron–Positron Collider, and proposed muon colliders—Compton scattering serves not only as a clean benchmark process for testing high-precision QED predictions, but also as a crucial tool for beam diagnostics, luminosity measurements, and polarization monitoring [5–8]. As these frontier facilities aim for unprecedented experimental precision, extraordinarily accurate theoretical predictions for Compton scattering become indispensable for fully exploiting their physics potential.

The total cross section of Compton scattering at leading order (LO) in QED was firstly calculated by Dirac [9], Gordon [10], and then by Klein and Nishina [11] with full spin and relativistic corrections. The next-to-leading order (NLO) QED correction has been studied both numerically and analytically [12–17], with the high-energy behavior being analyzed in [17–20]. It is found that the NLO correction is substantial, ranging from 8.2% at center-of-mass energy $\sqrt{s} = 1$ GeV to around 30% at $\sqrt{s} = 1$ TeV, which largely surpasses the expectation of normal perturbative expansion in QED, i.e., $\mathcal{O}(\alpha)$ with $\alpha \sim 1/137$ being the electromagnetic coupling.

This result can be understood from the analytical form of the total cross section at high energies [17],

$$\sigma_{\mathrm{tot}} \sim \frac{2\pi\alpha^2}{s} \ln\left(\frac{s}{m^2}\right)\left[1 + \frac{\alpha}{6\pi}\ln^2\left(\frac{s}{m^2}\right) + \cdots\right], \quad (1)$$

with m the electron mass. The double-logarithmic enhancement renders $\alpha\ln^2(s/m^2)$ of order $\mathcal{O}(1)$ at $\sqrt{s} \sim 1$ GeV, which eliminates the suppression of the coupling α at high orders. Consequently, the observed suppression at NLO stems purely from the $1/(6\pi)$ prefactor. This large logarithmic structure prompts two immediate questions: (i) whether the next-to-next-to-leading-order (NNLO) contribution still offers a significant improvement, and (ii) what

*Contact author: haitao.li@sdu.edu.cn
†Contact author: yqma@pku.edu.cn
‡Contact author: chengtaitan@stu.pku.edu.cn
§Contact author: j.wang@sdu.edu.cn
‖Contact author: hfzhang@mail.gufe.edu.cn

Published by the American Physical Society under the terms of the Creative Commons Attribution 4.0 International license. Further distribution of this work must maintain attribution to the author(s) and the published article's title, journal citation, and DOI. Funded by SCOAP³.

is the origin of these double logarithms and how can one resum them to all orders?

The double logarithms are usually related to uncancelled soft-collinear overlapping singularities. But the total cross section of Compton scattering is free of such singularities due to the Block-Nordsieck theorem [21]. Naïvely thinking, it only contains a singularity in the limit when the outgoing photon becomes collinear to the ingoing electron, a process called backward scattering. This corresponds to a Regge limit, i.e., $s \gg |t|$, which has been studied extensively [22–33]. The resummed leading logarithms (LLs) in the Regge limit studied in the above literatures, which concern Reggeized gluon exchange in QCD, take the form of $[\alpha_s \ln(s/(-t)]^n$. As such, they are not applicable to the double-logarithmic structure encountered in QED Compton scattering. We note that the double logarithmic terms in QED $2 \to 2$ processes at the amplitude level have been studied almost 60 years ago [34–36], which are, however, different from the result at the cross section level.

It is the purpose of this Letter to address the above two questions. We calculate the NNLO total cross section of Compton scattering by utilizing the modern multiloop techniques, which reveals further double logarithms at the high-energy limit. However, the leading logarithmic term is suppressed by a prefactor of $1/(96\pi^2)$. Based on the region analysis, we find that these logarithms emerge in the region with an exchange of a Glauber electron between a bunch of collinear and a bunch of anticollinear particles. The phase space and squared amplitude simplify significantly in this region so that we are able to predict the LLs at any order. The all-order structure clearly explains the suppressing prefactor through double factorial terms in the denominator, indicating rapid perturbative convergence for this process.

NNLO calculation—We focus on QED NNLO corrections to the total cross section of Compton scattering

$$e^-(p_1)\gamma(p_2) \to e^-(p_3)\gamma(p_4) \tag{2}$$

with full electron mass dependence. We do not consider contributions from final states with three charged particles because these processes can be separated experimentally. It is useful to define a dimensionless variable

$$\tau = \frac{m^2}{s} \tag{3}$$

with $s = (p_1 + p_2)^2$.

We employ FeynArts [37] to generate the Feynman amplitudes and use the CalcLoop package [38] to handle Lorentz and Dirac algebras, reduce squared amplitudes to linear combinations of scalar integrals, and map the latter to predefined integral families. To apply the modern multiloop calculation techniques, we have treated the phase space integrals as loop integrals by virtue of reverse unitarity [39–41]. The scalar integrals are then reduced to master integrals by using integration-by-part (IBP) identities [42] based on the Laporta algorithm [43]. We use the Blade package [44] to generate IBP identities and solve the IBP systems with the strategy of block-triangular form [45,46], employing FiniteFlow [47] as a solver. Finally, we construct the differential equations [48] of the master integrals with respect to τ. We use the dimensional regularization with $\epsilon = (4-d)/2$ to regulate both ultraviolet (UV) and infrared divergences. Instead of reconstructing the analytical ϵ dependence, we employ the strategy proposed in Refs. [49,50] to compute only a few ϵ points. In our calculation, we take the values as $\epsilon = -1/1000$ and $\epsilon = 1/1000$ [51], combination of which results in an error of $\mathcal{O}(10^{-6})$ at the cross section level.

We fix the boundary conditions of the master integrals by the auxiliary mass flow method [52–55] implemented in AMFlow [49]. In principle, one can choose an arbitrary regular point in the physical region. We choose $\tau = 1/530$ close to the high-energy endpoint $\tau = 0$, which is our primary concern. Then, all results of the master integrals in the physical region can be derived by solving the differential equations. Near the singular point $\tau = 0$, we directly solve the power series expansion [56,57] to extract the coefficients of all the logarithms $\ln^n\tau$, $n \le 5$. The Frobenius series solution for the differential equations of dimensionally regularized loop integrals has the form

$$f(\epsilon,\tau) = \sum_{a,b} \tau^a \ln^b(\tau) \left(\sum_{n=0}^{\infty} C_{abn}(\epsilon)\tau^n \right), \tag{4}$$

where b is a non-negative integer and a satisfies the pattern

$$a = a_0 + a_1\epsilon, \qquad 2a_0, a_1 \in Z. \tag{5}$$

The infrared divergences cancel after real and virtual contributions are combined together. The UV divergence is renormalized in the on-shell scheme. We adopt two methods to renormalize the bare cross sections. The first is to calculate the counterterm Feynman diagrams generated by FeynArts and the second is to replace the bare quantities with renormalized ones. In the second method, the bare results are multiplied with the coupling constant renormalization Z_α^{OS} and wave function renormalizations Z_2^{OS},Z_3^{OS} for the electron and photon, respectively. The bare electron mass in internal propagators is replaced with the on-shell mass $m^b = m^{\mathrm{OS}}(1+\delta_m)$. The needed renormalization constants can be found in Refs. [58,59]. After these manipulations, the cross section is expanded in the renormalized coupling constant α properly. The results of the two methods agree with each other.

At the end, the cross section in the full physical region $\tau \in (0,1)$ is obtained in terms of a piecewise power series with up to 16 segments. In each expansion point, we deeply expand the power series to guarantee the high precision of the numerical result. We check and confirm our result at another regular point $\tau = 49/53$ by direct numerical computation with AMFlow.

The total cross section near the threshold is given by

$$\sigma(x)=\frac{\pi\alpha^2}{m^2}\left(\frac{8}{3}-\frac{8}{3}x+\frac{52}{15}x^2-\frac{133}{30}x^3+\frac{572}{105}x^4\right)+\frac{\alpha^3}{m^2}x^2\left(-\frac{16}{9}\ln x+\frac{4}{3}x\ln x-\frac{25}{9}x^2\ln x\right.$$
$$\left.+\frac{7}{15}-\frac{113}{90}x+\frac{203}{125}x^2\right)+\frac{\alpha^4}{\pi m^2}x^2(0.814x^2\ln^2 x+0.797x^2\ln x-2.05+7.16x-18.6x^2)+\mathcal{O}(x^5), \quad (6)$$

where $x=(1-\tau)/\tau$. The higher-order corrections are vanishing due to the quadratic dependence on x. This is in concordance with Thirring's theorem [15,60,61], which provides a strong validation of our calculation. The above expression can be used to calculate the cross section when $0.9<\tau<1$.

At the high-energy limit, i.e., $\tau\leq 0.01$, we provide a deep expansion with a precision that is enough for experimental needs,

$$\sigma(\tau)=\frac{\pi\alpha^2}{s}[(2L+1)+\tau(-6L+17)+\tau^2(-30L+32)+\tau^3(-70L+48)+\tau^4(-126L+64)+\mathcal{O}(\tau^5)]$$
$$+\frac{\alpha^3}{s}\left[\left(\frac{1}{3}L^3-\frac{1}{2}L^2+\frac{17}{4}L-9.5016\right)+\tau(2L^3+13L^2-36.5340L+0.55139)+\right.$$
$$\left.+\tau^2\left(\frac{38}{3}L^3+\frac{151}{2}L^2-89.091L+47.062\right)+\tau^3\left(\frac{157}{3}L^3+\frac{344}{3}L^2-220.07L+149.73\right)+\mathcal{O}(\tau^4)\right]$$
$$+\frac{\alpha^4}{\pi s}\left[\left(\frac{1}{48}L^5-0.149L^4+1.34L^3-1.17L^2-16.6L+23.8\right)\right.$$
$$\left.+\tau(1.13L^5-6.54L^4-44.6L^3+442L^2-36.0L-2.64\times 10^3)+\mathcal{O}(\tau^2)\right], \quad (7)$$

with $L=\ln(1/\tau)$. The LO and NLO results agree with those given in [17], while the NNLO result is new. We indeed find a double-logarithmic enhancement at NNLO. Crucially, however, its leading-logarithmic coefficient is suppressed by a factor of $1/(96\pi^2)$, relative to the LO coefficient, significantly limiting its impact on the cross section. Numerically, the NNLO correction improves the NLO cross section by 0.2% at $\sqrt{s}=1$ GeV and 2.5% at $\sqrt{s}=1$ TeV, respectively.

For $0.01<\tau\leq 0.9$, we provide a list of numerical values in the auxiliary file, from which the NNLO correction can be computed using interpolation.

All-order leading logarithms—Now we derive the LL of Compton scattering in the high-energy limit to all orders. The logarithm at LO comes from the phase space integration of the t-channel diagram in the backward scattering limit. It can also be considered as the imaginary part of the corresponding forward scattering loop amplitude. Using the method of regions [62,63], we find four regions: the hard (h), collinear (c), anticollinear ($\bar{c}$), and soft (s) regions, as in the case of $H\to\gamma\gamma$ studied in Ref. [64]. Defining two light-cone directions n_-^μ and n_+^μ along the momenta p_1 and p_2, respectively, any momentum can be decomposed as $p^\mu=n_+pn_-^\mu/2+n_-pn_+^\mu/2+p_\perp^\mu=(n_+p,n_-p,p_\perp)$. The four regions correspond to the (t-channel electron) loop momentum q scaling as $\sqrt{s}(1,1,1)$, $\sqrt{s}(1,\lambda^2,\lambda)$, $\sqrt{s}(\lambda^2,1,\lambda)$, and $\sqrt{s}(\lambda,\lambda,\lambda)$, respectively, with the power counting parameter $\lambda=\sqrt{\tau}$.

Direct computation of the loop amplitude in the (anti) collinear and soft regions suffers from the problem of endpoint divergences. Imposing an analytic regulator $\nu^\eta/(n_+q+n_-q+i0)^\eta$ to regulate such divergences, we obtain the imaginary part from only the hard and anticollinear regions. Specifically, the hard and anticollinear region contributions combine in the form

$$\mathrm{Im}\left[\left(\frac{\mu^2}{-s-i0}\right)^\epsilon\frac{-1}{\epsilon^2}+\left(\frac{\mu^2}{m^2}\right)^\epsilon\left(\frac{\nu}{-\sqrt{s}+i0}\right)^\eta\frac{1}{\epsilon\eta}\right]$$
$$=-\pi\left[\ln\frac{\mu^2}{s}-\ln\frac{\mu^2}{m^2}\right]=-\pi\ln\tau. \quad (8)$$

This result explains the origin of the logarithmic structure clearly. However, it seems redundant to introduce the analytic regulator since we do not need the cancellation of $1/\eta$ poles as in other cases [64,65].

This regulator simply plays the role of inducing an imaginary part. Actually, the imaginary part can be obtained more intuitively from the unitarity of the S matrix. We employ the Cutkosky rule in the anticollinear region, forcing the photon propagator to be on shell, i.e., taking $\delta(n_-q\sqrt{s})$, which cancels the n_-q integration. The n_+q integration is also trivial due to the δ function associating with the on-shell electron propagator. Then the integral collapses to the perpendicular space $q_\perp$ integration, which generates the imaginary part in the second line of Eq. (8) directly. Therefore, applying the Cutkosky rule turns the

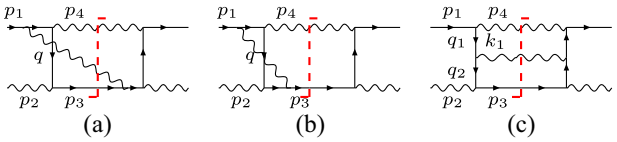

FIG. 1. NLO Feynman diagrams contributing to LLs, with (a) real photon emission, (b) virtual photon exchange, and (c) ladder diagram.

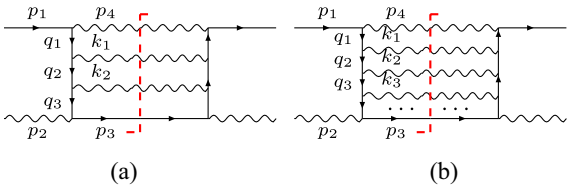

FIG. 2. Ladder diagrams at (a) NNLO and (b) all-order.

loop momentum q from an anticollinear mode into a Glauber mode (G), which scales as $\sqrt{s}(\lambda^2,\lambda^2,\lambda)$. In other words, the Glauber region is a subset of the anticollinear region. It is only this region that could yield an imaginary part [66].

At NLO, the extra double logarithm can usually be caused by the soft and collinear singularities induced by the additional real or virtual photon. If the additional photon is radiated from the external electrons, the double logarithms always cancel between the corresponding virtual and real corrections, which share the same topology; see an example in Figs. 1(a) and 1(b). Consequently, only the diagram with the additional photon emitted from the t-channel electron propagator, as shown in Fig. 1(c), could contribute to double logarithms. The full result of this diagram in the Feynman gauge is given by

$$\sigma^{\mathrm{NLO}}_{\mathrm{ladder}}=\frac{\alpha^3}{s}\left(\frac{L}{\epsilon}+\frac{1}{3}L^3+\frac{1}{2}L^2+L+\frac{5}{2}-\frac{2\pi^2}{3}-2\zeta_3+\mathcal{O}(\tau)\right). \tag{9}$$

The above IR divergence $1/\epsilon$ would cancel after including the renormalization of the electron wave function, which also contains IR divergences in the on-shell scheme.

The above LL is the same as that in the NLO total cross section in Eq. (7). The relevant regions for the imaginary part of the forward scattering amplitude consist of $(q_1,q_2)\sim(h,h),(c,h),(h,\bar{c}),(c,G),(G,\bar{c})$ with q_i the momenta of electron propagators; see Fig. 1(c). Note that the overlap of (c,G) and $(G,\bar{c})$ regions is nonvanishing and thus has to be subtracted. After finding all the contributing regions, one can set the scale $\mu=\sqrt{s}$ so that the regions containing h do not produce LLs. All the LLs come only from (c,G) or $(G,\bar{c})$ or their overlap. This judicious choice of scale would simplify the calculation a lot.

These structures can be extended to all orders. The t-channel electron momenta of the n-loop ladder diagram in the $\mathrm{N}^{n-1}\mathrm{LO}$ correction are labeled as $q_1,q_2,\ldots,q_n$, respectively, as shown in Fig. 2. We adopt the notation $r_i=(c,\ldots,c,G,\bar{c},\ldots,\bar{c})$ to denote the region where $q_j(j<i)$ and $q_k(k>i)$ are collinear and anticollinear, respectively, while q_i is a Glauber mode. The momenta of final-state photons are denoted by $k_i, i=0,\ldots,n-1$, with $k_0=p_4$. Momentum conservation requires $k_i=q_i-q_{i+1}$ with $q_0=p_1$, and $p_3=q_n+p_2$. The LL arises when the light-cone momentum components obey the strong ordering

$$n_+q_0>n_+q_1>\cdots>n_+q_n>0, \tag{10a}$$

$$0<-n_-q_1<\cdots<-n_-q_n<n_-p_2. \tag{10b}$$

The first equation (10a) always holds since $n_\pm k_i>0$ and $k_i^2=0$, while the second equation (10b) helps chisel out the subregion contributing to LLs. It is easy to check that this subregion is contained in any of the r_i regions. Therefore, all r_i regions as well as any overlap give the same result.

The $(n+1)$-body phase space can be written as

$$\int \mathrm{dPS}_{n+1}=(2\pi)\int\prod_{i=1}^{n}\frac{\mathrm{d}^4q_i}{(2\pi)^3}\delta^+(p_3^2-m^2)\prod_{j=0}^{n-1}\delta^+(k_j^2)$$

with $\delta^+(p^2)=\delta(p^2)\theta(p^0)$. Based on the strong ordering in (10) and a useful trick in dealing with LLs, i.e., dropping the smaller component in an expression, the on-shell conditions are given by $\delta(k_0^2)\approx\delta((n_+q_0)(n_-q_0-n_-q_1)-q_{1T}^2)$, $\delta(k_i^2)\approx\delta(-(n_+q_i)(n_-q_{i+1})-(q_i-q_{i+1})_T^2), i=1,\ldots,n-1$, and $\delta(p_3^2-m^2)\approx\delta(n_+q_nn_-p_2-q_{nT}^2-m^2)$, which render the integrations of n_-q_i $(i=1,\ldots,n)$ and n_+q_n trivial. Simultaneously, the squared amplitude is also simplified with the denominators $q_i^2-m^2\approx-q_{iT}^2-m^2-(n_+q_i/n_+q_{i-1})q_{(i-1)T}^2$. Defining the variables $x_i=n_+q_i\sqrt{s}/m^2$ and $y_i=(q_{iT}^2+m^2)/m^2$, the LL in the cross section is given by

$$\sigma^{\mathrm{N}^{n-1}\mathrm{LO}}_{\mathrm{LL}}=\frac{4\pi^2}{s}\frac{\alpha^{n+1}}{(2\pi)^n}\int_1^{1/\tau}\frac{\mathrm{d}x_1}{x_1}\prod_{j=2}^{n-1}\int_1^{x_{j-1}}\frac{\mathrm{d}x_j}{x_j}\times\int_1^{x_1}\frac{\mathrm{d}y_1}{y_1}\prod_{i=2}^{n-1}\int_{\max\{1,\frac{x_i}{x_{i-1}}y_{i-1}\}}^{x_i}\frac{\mathrm{d}y_i}{y_i}\int_1^{x_{n-1}}\frac{\mathrm{d}y_n}{y_n}, \tag{11}$$

where we have replaced the dimensional regularization of the divergences by a cutoff regularization. The lower bound of x_j and upper bound of y_j with $j=1,\ldots,n-1$ are determined since q_j is supposed to be a collinear momentum. The upper bound of y_n is set because of $y_n=x_n<x_{n-1}$. The other bounds can be understood easily. These $2n-1$ fold integrations generate the $(2n-1)$-th powers of logarithms. The nonladder diagrams do not have this recursive structure and thus contain no LLs.

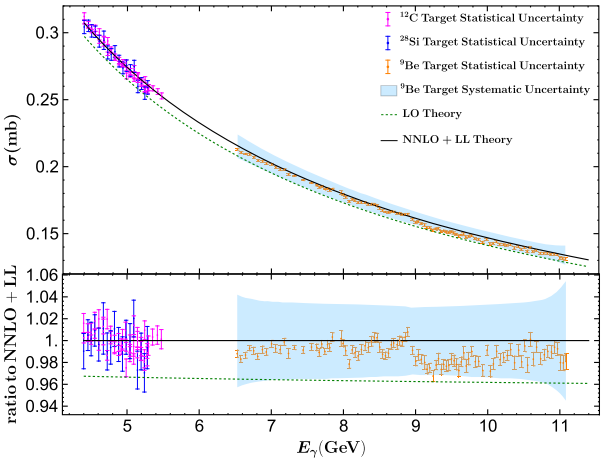

FIG. 3. Comparison of theory and experiment for Compton scattering. PrimEx [67] (4.400–5.475 GeV) and GlueX [68] (6.5–11.1 GeV) data for ^{12}C (magenta), ^{28}Si (blue), and ^{9}Be (orange) are compared to theoretical predictions at LO (green dashed) and NNLO + LL (black solid). The NLO result is not shown as it is visually identical to NNLO + LL.

Evaluating the above integral leads to the result

$$\sigma_{\mathrm{LL}}^{\mathrm{N}^{n-1}\mathrm{LO}} = -\frac{2\alpha^{n+1}}{(2\pi)^{n-2}s}\frac{1}{(n-1)!(n+1)!}\ln^{2n-1}\tau. \quad (12)$$

This formula agrees with the NLO and NNLO results in Eq. (7). To further validate the result, we calculated the NNNLO ladder diagram using the multiloop techniques described above, and found full agreement. The double factorials in the denominator lead to a strong numerical suppression at high orders, explaining why NNLO contributions are not so prominent for Compton scattering in the high-energy limit where large logarithmic enhancement exists.

Summing the all order corrections, we obtain the LLs resummed cross section

$$\begin{aligned}\sigma_{\mathrm{LL}} &= -\frac{8\pi^2\alpha}{s\ln\tau}I_2\left(\sqrt{\frac{2\alpha}{\pi}}\ln\tau\right)\\ &= \frac{2^{9/4}\pi^{7/4}\alpha^{3/4}}{s(-\ln\tau)^{3/2}\tau\sqrt{2\alpha/\pi}} \quad \text{as } \tau\to 0, \end{aligned} \quad (13)$$

with $I_2(z)$ being the modified Bessel function of the first kind. In the second line of the above equation, we present the asymptotic expansion of the resummed result in the limit of $\tau \to 0$. For fixed m, the cross section is scaling as $s^{-1+\sqrt{2\alpha/\pi}}/\ln^{3/2}(s/m^2)$ as $s\to\infty$, a pattern in contrast to the Regge trajectory. On the other hand, the cross section becomes divergent as $m\to 0$ for fixed s since new infrared divergences would emerge in this limit.

Comparison with data—The strong suppression of LLs at higher orders ensures that our combined NNLO + resummation result provides an exceptionally precise prediction for the Compton-scattering cross section. This is demonstrated phenomenologically in Fig. 3, where we compare our most precise theoretical prediction with high-precision data from the PrimEx [67] and GlueX [68] collaborations using photons with energies of 4.400–5.475 GeV and 6.5–11.1 GeV, respectively. The numerical values of the fine-structure constant and electron mass are taken from precise measurements of [69] and [70], i.e., $\alpha = 1/137.035999$ and $m_e = 0.509108$ MeV. The theory and data show excellent agreement. We emphasize that the combined NNLO and resummation effects are minuscule (at the 0.05% level) in this energy regime, underscoring the rapid convergence of the perturbative QED series and the definitive nature of our prediction.

Summary—We have performed a precision study of the Compton-scattering total cross section, resolving the long-standing puzzle of the size of high-order corrections, particularly the role of high-energy double logarithms. Our calculation, which provides the first complete NNLO result with full electron mass dependence, reveals that the anticipated double-logarithmic enhancement is indeed present but numerically suppressed due to a small coefficient, leading to excellent perturbative convergence.

We traced the origin of these logarithms to a specific kinematic configuration induced by a Glauber electron exchange. This insight allowed us to resum the leading logarithmic contributions to all orders in perturbation theory, yielding a compact result expressed in terms of a modified Bessel function. The all-order analysis uncovers a suppression mechanism: double factorial terms in the denominator systematically dampen the leading logarithms. The combination of our NNLO calculation and all-orders resummation delivers a precise QED prediction, which we have validated against recent high-precision data from the PrimEx and GlueX collaborations.

The methodology developed here—particularly the identification of Glauber-type exchanges as the source of leading logarithms—opens a new avenue for high-precision calculations in other fundamental processes. This approach is directly applicable to processes like $e^+e^-\to\gamma\gamma$ and $gg\to t\bar{t}$ in the high-energy limit, where similar logarithmic structures arise from massive fermion exchanges. Our Letter thus provides a blueprint for achieving percent-level precision in a range of scattering processes at future colliders.

The diagrams are drawn using TikZ-Feynman [71].

Acknowledgments—We would like to thank Jia-Yang Dong, Kirill Kudashkin, and Da-Jiang Zhang for the useful discussion and collaboration on similar projects. The work was supported in part by the National Natural Science Foundation of China (Grants No. 12565012, No. 12325503, No. 12321005, No. 12275156, and No. 12005117) and the High-performance Computing Platform of Peking University.

Data availability—The data that support the findings of this article are openly available [72].

[1] A. H. Compton, A quantum theory of the scattering of x-rays by light elements, Phys. Rev. **21**, 483 (1923).
[2] M. Mahesh, The essential physics of medical imaging, third edition, Med. Phys. **40**, 077301 (2013).
[3] V. Schoenfelder *et al.*, Instrument description and performance of the imaging gamma-ray telescope COMPTEL aboard the Compton gamma-ray observatory, Astrophys. J. Suppl. Ser. **86**, 657 (1993).
[4] I. Tkachev, S. Musin, D. Abdurashitov, A. Baranov, F. Guber, A. Ivashkin, and A. Strizhak, Measuring the evolution of entanglement in Compton scattering, Sci. Rep. **15**, 6064 (2025).
[5] G. Aarons *et al.*, ILC reference design report volume 3—accelerator, arXiv:0712.2361.
[6] A. Abada *et al.* (FCC Collaboration), FCC-ee: The lepton collider: Future circular collider conceptual design report volume 2, Eur. Phys. J. Spec. Top. **228**, 261 (2019).
[7] CEPC Study Group, CEPC conceptual design report: Volume 1—accelerator, arXiv:1809.00285.
[8] J. P. Delahaye, M. Diemoz, K. Long, B. Mansoulié, N. Pastrone, L. Rivkin, D. Schulte, A. Skrinsky, and A. Wulzer, Muon colliders, arXiv:1901.06150.
[9] P. A. M. Dirac, Relativity quantum mechanics with an application to Compton scattering, Proc. R. Soc. A **111**, 405 (1926).
[10] W. Gordon, Der Comptoneffekt nach der Schrödingerschen Theorie, Z. Phys. **40**, 117 (1926).
[11] O. Klein and Y. Nishina, Über die Streuung von Strahlung durch freie Elektronen nach der neuen relativistischen Quantendynamik von Dirac, Z. Phys. **52**, 853 (1929).
[12] L. M. Brown and R. P. Feynman, Radiative corrections to Compton scattering, Phys. Rev. **85**, 231 (1952).
[13] F. Mandl and T. H. R. Skyrme, The theory of the double Compton effect, Proc. R. Soc. A **215**, 497 (1952).
[14] M. L. Swartz, A Complete order α^3 calculation of the cross-section for polarized Compton scattering, Phys. Rev. D **58**, 014010 (1998).
[15] A. Denner and S. Dittmaier, Complete $O(\alpha)$ QED corrections to polarized Compton scattering, Nucl. Phys. **B540**, 58 (1999).
[16] R. N. Lee, A. A. Lyubyakin, and V. A. Stotsky, Total cross sections of $e\gamma \to eX\bar{X}$ processes with $X = \mu$, γ, e via multiloop methods, J. High Energy Phys. 01 (2021) 144.
[17] R. N. Lee, M. D. Schwartz, and X. Zhang, Compton scattering total cross section at next-to-leading order, Phys. Rev. Lett. **126**, 211801 (2021).
[18] M. Gell-Mann, M. Goldberger, F. Low, E. Marx, and F. Zachariasen, Elementary particles of conventional field theory as Regge poles. III, Phys. Rev. **133**, B145 (1964).
[19] B. M. McCoy and T. T. Wu, Theory of fermion exchange in massive quantum electrodynamics at high-energy. I, Phys. Rev. D **13**, 369 (1976).
[20] A. Sen, Asymptotic behavior of the fermion and gluon exchange amplitudes in massive quantum electrodynamics in the Regge limit, Phys. Rev. D **27**, 2997 (1983).
[21] F. Bloch and A. Nordsieck, Note on the radiation field of the electron, Phys. Rev. **52**, 54 (1937).
[22] C. Frye, H. Hannesdottir, N. Paul, M. D. Schwartz, and K. Yan, Infrared finiteness and forward scattering, Phys. Rev. D **99**, 056015 (2019).
[23] H. Hannesdottir and M. D. Schwartz, S -matrix for massless particles, Phys. Rev. D **101**, 105001 (2020).
[24] H. Hannesdottir and M. D. Schwartz, Finite S matrix, Phys. Rev. D **107**, L021701 (2023).
[25] V. Del Duca and E. W. N. Glover, The high-energy limit of QCD at two loops, J. High Energy Phys. 10 (2001) 035.
[26] V. Del Duca, G. Falcioni, L. Magnea, and L. Vernazza, High-energy QCD amplitudes at two loops and beyond, Phys. Lett. B **732**, 233 (2014).
[27] V. Del Duca, G. Falcioni, L. Magnea, and L. Vernazza, Analyzing high-energy factorization beyond next-to-leading logarithmic accuracy, J. High Energy Phys. 02 (2015) 029.
[28] V. Del Duca, C. Duhr, E. Gardi, L. Magnea, and C. D. White, The infrared structure of gauge theory amplitudes in the high-energy limit, J. High Energy Phys. 12 (2011) 021.
[29] G. Pancheri and Y. N. Srivastava, Introduction to the physics of the total cross-section at LHC: A review of data and models, Eur. Phys. J. C **77**, 150 (2017).
[30] L. N. Lipatov, Reggeization of the vector meson and the vacuum singularity in nonAbelian gauge theories, Sov. J. Nucl. Phys. **23**, 338 (1976), https://inspirehep.net/literature/113228.
[31] E. A. Kuraev, L. N. Lipatov, and V. S. Fadin, Multiregge processes in the Yang-Mills theory, Sov. Phys. JETP **44**, 443 (1976), https://inspirehep.net/literature/116034.
[32] V. S. Fadin, E. A. Kuraev, and L. N. Lipatov, On the pomeranchuk singularity in asymptotically free theories, Phys. Lett. **60B**, 50 (1975).
[33] I. I. Balitsky and L. N. Lipatov, The pomeranchuk singularity in quantum chromodynamics, Sov. J. Nucl. Phys. **28**, 822 (1978), https://inspirehep.net/literature/137229.
[34] V. G. Gorshkov, V. N. Gribov, L. N. Lipatov, and G. V. Frolov, Double logarithmic asymptotics of quantum electrodynamics, Phys. Lett. **22**, 671 (1966).
[35] V. G. Gorshkov, V. N. Gribov, L. N. Lipatov, and G. V. Frolov, Doubly logarithmic asymptotic behavior in quantum electrodynamics, Yad. Fiz. **6**, 129 (1967), https://inspirehep.net/literature/50148.
[36] V. G. Gorshkov, V. N. Gribov, L. N. Lipatov, and G. V. Frolov, Backward electron—positron scattering at high-energies, Yad. Fiz. **6**, 361 (1967), https://inspirehep.net/literature/50149.
[37] T. Hahn, Generating Feynman diagrams and amplitudes with FeynArts 3, Comput. Phys. Commun. **140**, 418 (2001).
[38] https://e.gitee.com/multiloop-pku/repos/multiloop-pku/calcloop/sources.
[39] C. Anastasiou and K. Melnikov, Higgs boson production at hadron colliders in NNLO QCD, Nucl. Phys. **B646**, 220 (2002).
[40] C. Anastasiou, L. J. Dixon, and K. Melnikov, NLO Higgs boson rapidity distributions at hadron colliders, Nucl. Phys. B, Proc. Suppl. **116**, 193 (2003).
[41] C. Anastasiou, L. J. Dixon, K. Melnikov, and F. Petriello, Dilepton rapidity distribution in the Drell-Yan process at NNLO in QCD, Phys. Rev. Lett. **91**, 182002 (2003).

[42] K. G. Chetyrkin and F. V. Tkachov, Integration by parts: The algorithm to calculate β-functions in 4 loops, Nucl. Phys. **B192**, 159 (1981).
[43] S. Laporta, High-precision calculation of multiloop Feynman integrals by difference equations, Int. J. Mod. Phys. A **15**, 5087 (2000).
[44] X. Guan, X. Liu, Y.-Q. Ma, and W.-H. Wu, Blade: A package for block-triangular form improved Feynman integrals decomposition, Comput. Phys. Commun. **310**, 109538 (2025).
[45] X. Liu and Y.-Q. Ma, Determining arbitrary Feynman integrals by vacuum integrals, Phys. Rev. D **99**, 071501 (2019).
[46] X. Guan, X. Liu, and Y.-Q. Ma, Complete reduction of integrals in two-loop five-light-parton scattering amplitudes, Chin. Phys. C **44**, 093106 (2020).
[47] T. Peraro, FiniteFlow: Multivariate functional reconstruction using finite fields and dataflow graphs, J. High Energy Phys. 07 (2019) 031.
[48] A. V. Kotikov, Differential equations method: New technique for massive Feynman diagrams calculation, Phys. Lett. B **254**, 158 (1991).
[49] X. Liu and Y.-Q. Ma, AMFlow: A Mathematica package for Feynman integrals computation via auxiliary mass flow, Comput. Phys. Commun. **283**, 108565 (2023).
[50] X. Chen, X. Guan, C.-Q. He, X. Liu, and Y.-Q. Ma, Heavy-quark pair production at lepton colliders at NNNLO in QCD, Phys. Rev. Lett. **132**, 101901 (2024).
[51] H.-Y. Bi, L.-H. Huang, R.-J. Huang, Y.-Q. Ma, and H.-M. Yu, Electroweak corrections to double Higgs production at the LHC, Phys. Rev. Lett. **132**, 231802 (2024).
[52] X. Liu, Y.-Q. Ma, and C.-Y. Wang, A systematic and efficient method to compute multi-loop master integrals, Phys. Lett. B **779**, 353 (2018).
[53] X. Liu, Y.-Q. Ma, W. Tao, and P. Zhang, Calculation of Feynman loop integration and phase-space integration via auxiliary mass flow, Chin. Phys. C **45**, 013115 (2021).
[54] X. Liu and Y.-Q. Ma, Multiloop corrections for collider processes using auxiliary mass flow, Phys. Rev. D **105**, L051503 (2022).
[55] Z.-F. Liu and Y.-Q. Ma, Determining Feynman integrals with only input from linear algebra, Phys. Rev. Lett. **129**, 222001 (2022).
[56] M. Caffo, H. Czyz, M. Gunia, and E. Remiddi, BOKASUN: A fast and precise numerical program to calculate the master integrals of the two-loop sunrise diagrams, Comput. Phys. Commun. **180**, 427 (2009).
[57] M. Czakon, Tops from light quarks: Full mass dependence at two-loops in QCD, Phys. Lett. B **664**, 307 (2008).
[58] D. J. Broadhurst, N. Gray, and K. Schilcher, Gauge invariant on-shellZ_2 in QED, QCD and the effective field theory of a static quark, Z. Phys. C **52**, 111 (1991).
[59] K. Melnikov and T. van Ritbergen, The three loop on-shell renormalization of QCD and QED, Nucl. Phys. **591B**, 515 (2000).
[60] W. E. Thirring, Radiative corrections in the nonrelativistic limit, Philos. Mag. Ser. 7 **41**, 1193 (1950).
[61] S. Dittmaier, Thirring's low-energy theorem and its generalizations in the electroweak standard model, Phys. Lett. B **409**, 509 (1997).
[62] V. A. Smirnov, Asymptotic expansions of two loop Feynman diagrams in the Sudakov limit, Phys. Lett. B **404**, 101 (1997).
[63] M. Beneke and V. A. Smirnov, Asymptotic expansion of Feynman integrals near threshold, Nucl. Phys. **B522**, 321 (1998).
[64] J.-Y. Hou, J. Wang, and D.-J. Zhang, Region analysis of $H \to \gamma\gamma$ via a bottom quark loop, J. High Energy Phys. 06 (2025) 164.
[65] G. Bell, P. Böer, and T. Feldmann, Muon-electron backward scattering: A prime example for endpoint singularities in SCET, J. High Energy Phys. 09 (2022) 183.
[66] J. F. Donoghue, B. K. El-Menoufi, and G. Ovanesyan, Regge behavior in effective field theory, Phys. Rev. D **90**, 096009 (2014).
[67] P. Ambrozewicz *et al.* (PrimEx Collaboration), High precision measurement of Compton scattering in the 5 GeV region, Phys. Lett. B **797**, 134884 (2019).
[68] F. Afzal *et al.* (GlueX Collaboration), Measurement of the total Compton scattering cross section between 6.5 and 11 GeV, Phys. Lett. B **870**, 139914 (2025).
[69] R. H. Parker, C. Yu, W. Zhong, B. Estey, and H. Müller, Measurement of the fine-structure constant as a test of the standard model, Science **360**, 191 (2018).
[70] S. Sturm, F. Köhler, J. Zatorski, A. Wagner, Z. Harman, G. Werth, W. Quint, C. H. Keitel, and K. Blaum, High-precision measurement of the atomic mass of the electron, Nature (London) **506**, 467 (2014).
[71] J. Ellis, TikZ-Feynman: Feynman diagrams with TikZ, Comput. Phys. Commun. **210**, 103 (2017).
[72] H. T. Li, Y.-Q. Ma, C.-T. Tan, J. Wang, and H.-F. Zhang, arXiv:2511.09330.